PCCP

Synthesis, structure and surface properties of some mesoporous cero-phosphoro-aluminates

E. K. Galanos,[a] D. E. Petrakis,*[a] V. N. Stathopoulos,[a] P. J. Pomonis,[a] D. P. Labou[b] and A. T. Sdoukos[a]

[a] *Department of Chemistry, University of Ioannina, Ioannina 45110, Greece. E-mail: dpetraki@cc.uoi.gr*
[b] *FORTH-ICE/HT, P.O. BOX 1414, 26500, Patras, Greece*

Received 6th February 2002, Accepted 1st May 2002
First published as an Advance Article on the web 18th June 2002

Mesoporous cero-phosphoro-aluminates ($Al_{100}P_XCe_Y$, X, $Y = 0$, 5, 10, 20) have been prepared and characterized by XRD analysis, surface area and porosity measurements, XPS analysis and surface acidity determination. The preparation of the $Al_{100}P_XCe_Y$ solids took place in an aqueous environment with NH_3 as precipitating agent and heating at 600 °C. The addition of phosphorus leads to an increase in the specific surface area (SSA) of the γ-Al_2O_3 parent solid from 230 to 390 $m^2\ g^{-1}$ and the formation of amorphous aluminophosphates. The addition of cerium does not result in its incorporation into the alumina or the aluminophosphate solids but a separate phase of CeO_2 is formed at $X, Y < 20$ while at $X, Y = 20$ $CePO_4$ becomes apparent. At the same time the specific surface area drops from 230–390 $m^2\ g^{-1}$ to 170–180 $m^2\ g^{-1}$ depending on the sample. All the $Al_{100}P_XCe_Y$ samples are truly mesoporous with mean pore diameters around 6–10 nm and full width at half maximum (FWHM) of the pore size distribution at 3–7 nm. The size of the crystallites of CeO_2 (Sherrer relationship) is around 4–8 nm depending on the sample. The surface acid density, determined by NH_3 adsorption, increases linearly with the addition of phosphates from 5×10^{17} sites m^{-2} for X = 0 to 13×10^{17} sites m^{-2} for $X = 20$, while it is practically invariant on addition of cerium. The XPS analysis showed that the surface of those porous materials is highly enriched in cerium as compared to the nominal solid composition. The enrichment is more substantial in pure alumina, reaching relative values of 100–150%, and decreases with the addition of phosphorus, where the relative enrichment is 30–60%. The surface of the solids without or with the addition of a small amount of cerium ($Y = 0$,5,10) is moderately enriched in phosphorus (10–30%) while for high cerium content ($Y = 20$) the surface is moderately depleted of phosphorus to 14–23%. The surface enrichment, or depletion, in phosphorus and/or cerium is corroborated by linear relationships between the surface composition (XPS) and the acidity (TPD NH_3) in the case of phosphorus or the intensity of the main reflection in XRD of CeO_2 in the case of cerium.

Introduction

Cerium oxide in pure form and cerium oxide containing other materials have been under intense scrutiny as components of heterogeneous catalysts, mainly for redox reactions.[1] The impetus of this research came from the realization that CeO_2 is a valuable component of three-way-catalysts[2–4] but it is also used as a component of several oxidation catalysts,[5–10] for removal of SO_x from fluid catalytic cracking flue gases[11] and as an additive in various green fuels. The beneficial action of CeO_2 stems mainly from its ability to undergo easily reduction–oxidation cycles, *i.e.* storing oxygen under oxidative conditions and releasing it under reductive conditions[12–16] $CeO_2 \rightleftharpoons Ce_2O_3$. Another noticeable effect of CeO_2 is the better dispersion of precious metals on supports, mostly Al_2O_3,[17–24] and the modification of the corresponding metal–support bonds and interactions. It has been also noticed that the presence of CeO_2 increases the mechanical strength of Al_2O_3[25] and stabilizes its thermal loss[26,27] by preventing the transformation of γ-Al_2O_3 to α-Al_2O_3. In another recent work,[28] addition of CeO_2 to Al_2O_3 resulted in (i) enhanced acidity of the surface Ce^{+4} sites and the Al^{+3} Lewis sites and (ii) induction in the alumina network of an altered porous texture. Nevertheless there has been no experimental study of to what extent cerium or phosphorus are accumulated on the surface of alumino-phosphoro-cerates and how the acidity and porosity are interrelated in such materials. The question of surface area in such systems is critical, since it is directly related to the reducibility of the surface CeO_2.[29] Moreover, the acid–base sites are important for the adsorption of hydrocarbons, since the existence of strong acid sites on ceria is believed to be important in the activation of hydrocarbons at high temperatures *via* H-abstraction.[30]

This paper addresses the question of surface area, porosity, acidity and surface composition of Al_2O_3/CeO_2 and $Al_2O_3/CeO_2/PO_4$ systems. The addition of phosphates was considered a critical factor for testing since, as has been shown in the past,[31–35] their presence in alumina-based solids influences both the porosity and surface area as well as the acidity. On the other hand, ceria is considered to be a basic substance and its combination with acidic phosphates can influence the surface catalytic activity and/or selectivity of such solids.

Experimental

Preparation of specimens

The samples examined had the general formula $Al_{100}P_XCe_Y$-600 where X, $Y = 0$, 5, 10, 20 and 600 was the final firing temperature. The parameters X and Y correspond to atoms in the

 DOI: 10.1039/b201310j

solids, the balance being oxygen. The preparation took place as follows: The calculated amounts of $Al(NO_3)_3{\cdot}9H_2O$ (Merck, p.a.), $Ce(NO_3)_3{\cdot}6H_2O$ (Aldrich) and H_3PO_4 (Ferak, p.a.) were dissolved in 250 ml of distilled water. The preparation took place by starting with a fixed amount (g) of $Al(NO)_3{\cdot}9H_2O$ and adding variable amounts of $Ce(NO)_3{\cdot}6H_2O$ and of H_3PO_4. The last reagent was taken from a concentrated solution of commercial H_3PO_4 85 wt.% and diluted to 0.75 M, the final concentration was checked by titration with 0.1 M NaOH. Then NH_4OH (Ferak, p.a.) was added gradually under stirring to pH 9.5. The formed gel was dried at 110 °C for 24 h. Since thermogravimetric studies showed that such gels lose mass around 300–350 °C and stabilise their weight above this temperature, the heating at this region took place very slowly in a tubular furnace under atmospheric conditions. The final firing temperature was set to 600 °C for a 6 h period. The sixteen samples prepared and some of their properties are listed in Table 1.

XRD

The XRD patterns of the dried samples were recorded using a SIEMENS diffract 500 automatic diaffractometer at 298 K employing Cu-Kα radiation ($\lambda = 1.5418$ Å). The results are shown in Fig. 1.

Surface area and porosity

The surface area and pore size distribution measurements were carried out using a Fisons Sorptomatic 1900 instrument. The characterisation techniques included the determination of nitrogen adsorption–desorption isotherms at 77 K from which the pore size distributions were determined, using the BJH method in the desorption branch, and are shown in Fig. 2. The calculated specific surface areas (BET), the pore volumes (BJH) as well as the mean pore diameters are cited in Table 1 and their variation as a function of phosphorus and cerium is given in Fig. 3(a)–(c).

Surface acidity

The surface acidity of the prepared solids was determined by temperature programmed desorption (TPD) of NH_3 in a flow system. Each sample (*ca.* 350 mg) was placed on the perforated bed of a silica tube of 0.5 cm internal diameter and heated externally by a tubular furnace. A temperature programme enabled the temperature to be increased in a controlled manner. The adsorption–desorption cell was connected to a Shimadzu gas chromatograph equipped with a thermal conductivity detector (TCD) to record the evolved gases. The gaseous outflow was passed through a trap

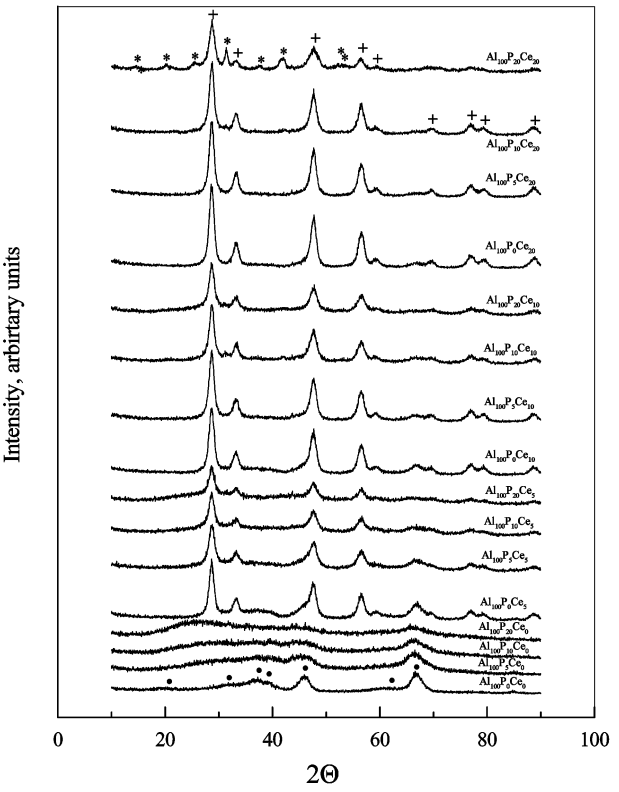

Fig. 1 XRD patterns of the Al–P–Ce–O mesoporous solids heated at 600 °C. (●) γ-Al_2O_3, (+) CeO_2, (*) $CePO_4$.

Table 1 Surface area, pore volume and pore sizes of $Al_{100}P_XCe_Y$ solids. The acidity of the samples is also shown per g and per m^2

Sample	Surface area S BET/m^2 g^{-1}	Pore volume V_p BJH/cm^3 g^{-1}	Mean pore diameter ($d_p = 4V_p/S$)/nm	Acid sites per g/$\times 10^{-20}$	Acid sites per m/$\times 10^{-17}$
$Al_{100}P_0Ce_0$	233.74	0.393	6.73	1.231	5.268
$Al_{100}P_5Ce_0$	386.22	0.735	7.61	3.261	8.444
$Al_{100}P_{10}Ce_0$	390.17	0.908	9.31	3.655	9.369
$Al_{100}P_{20}Ce_0$	321.98	0.849	10.55	4.049	12.577
$Al_{100}P_0Ce_5$	192.55	0.318	6.61	1.006	5.222
$Al_{100}P_5Ce_5$	260.79	0.394	6.04	2.251	7.760
$Al_{100}P_{10}Ce_5$	318.95	0.932	11.69	2.988	10.120
$Al_{100}P_{20}Ce_5$	234.97	0.916	15.59	3.325	14.150
$Al_{100}P_0Ce_{10}$	176.96	0.284	6.42	0.294	5.223
$Al_{100}P_5Ce_{10}$	228.37	0.458	8.02	1.963	8.594
$Al_{100}P_{10}Ce_{10}$	230.64	0.604	10.48	2.287	9.918
$Al_{100}P_{20}Ce_{10}$	254.59	1.010	15.87	2.525	12.600
$Al_{100}P_0Ce_{20}$	167.54	0.269	6.42	0.811	4.843
$Al_{100}P_5Ce_{20}$	208.70	0.291	5.58	1.736	8.318
$Al_{100}P_{10}Ce_{20}$	210.16	0.326	6.20	1.877	8.931
$Al_{100}P_{20}Ce_{20}$	183.29	0.375	8.18	2.027	11.057

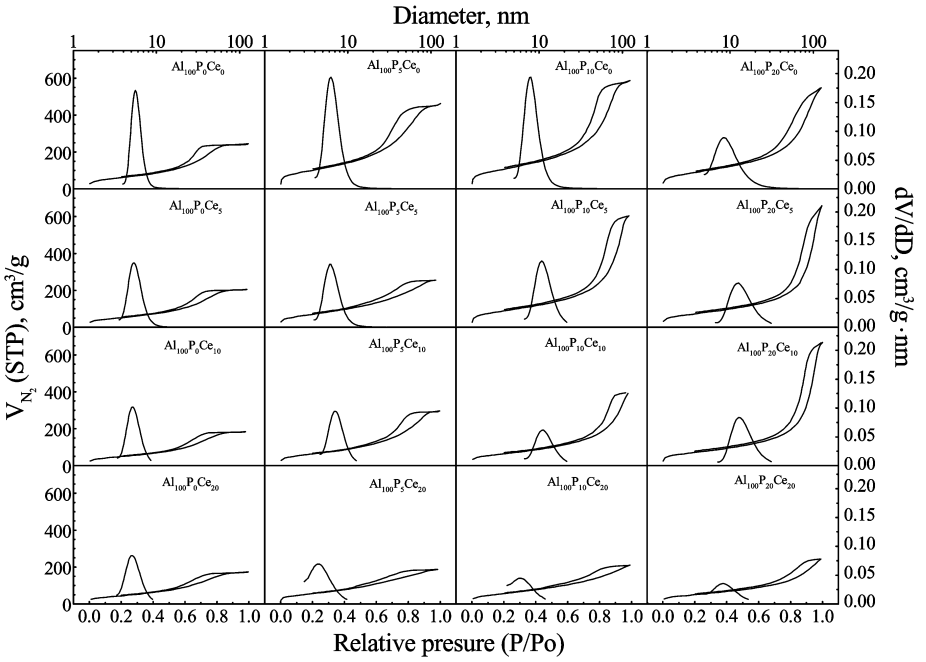

Fig. 2 Adsorption–desorption isotherms (77 K) of Al–P–Ce–O mesoporous solids and the corresponding pore size distribution (BJH).

containing a known amount of 0.01 M HCl. The experiments took place as follows: the solids were initially degassed *in situ* by heating them for 2 h at 500 °C in a flow of 50 cm^3 min^{-1} of He. The temperature was dropped to 100 °C and an ammonia stream was forced slowly through the sample for 0.5 h at 1.5 bar. Then the flow of ammonia was stopped and the system was switched again to He. The temperature was raised slightly to 105 °C in order to remove any excess NH_3 trapped in the cell. This stripping process lasted for 1 h. Then the desorption was started by increasing the temperature of the furnace at a rate of 10 °C min^{-1} to 500 °C. The desorbed NH_3 was recorded in the GC and the signals obtained are shown in Fig. 4. The total amount of NH_3 desorbed and trapped in the HCl was calculated by titration of the excess HCl with NaOH (0.01 M). Each NH_3 molecule is considered to correspond to one surface acid site. The results calculated in terms of acid sites g^{-1} and as acid sites m^{-2} are shown as a function of phosphorus concentration in Fig. 3(d) and (e).

XPS

The surface composition of $Al_{100}P_XCe_Y$ solids was determined by eans of X-ray photoelectron spectroscopy (XPS). The

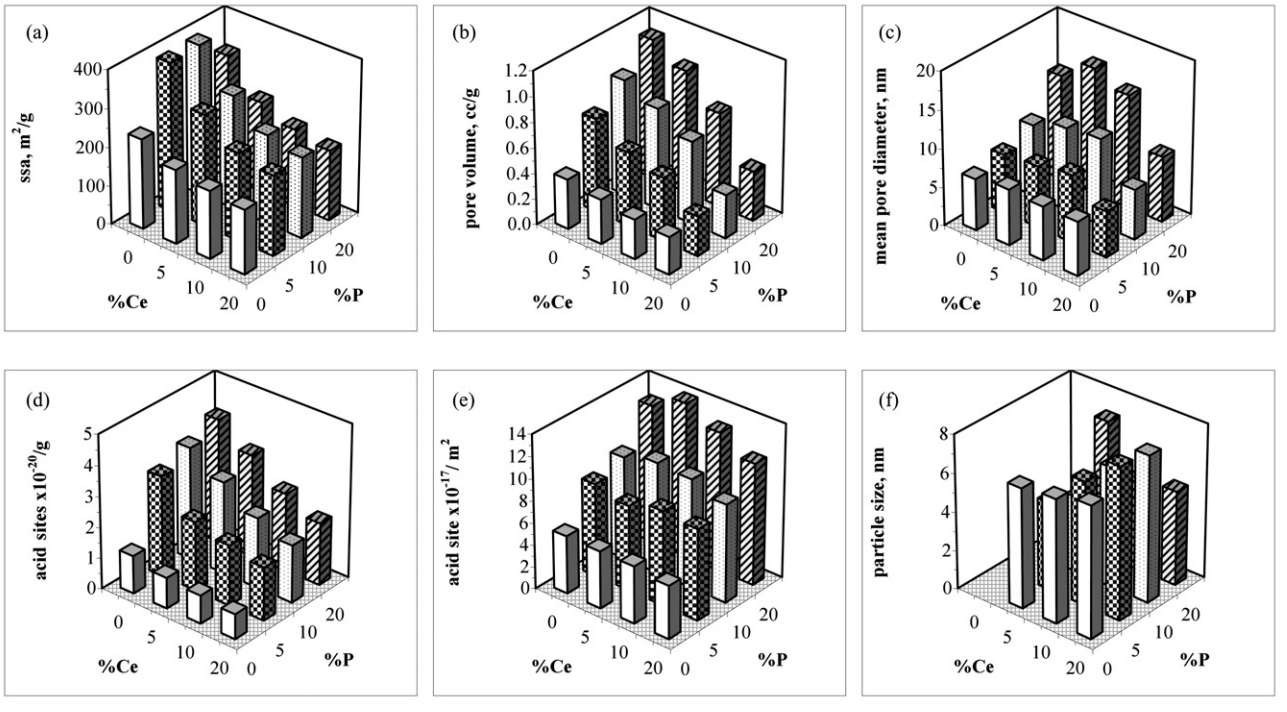

Fig. 3 Variation of the specific surface area (a), the pore volume (b), mean pore diameter (c), the surface acidity of the Al–P–Ce–O solids per g (d) and per m^2 (e) as well as the size of CeO_2 crystallites (f) calculated *via* the Sherrer relationship.

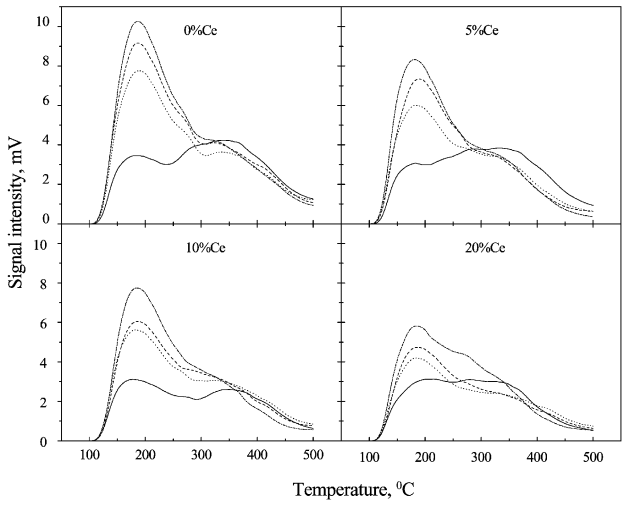

Fig. 4 NH_3 TPD signals of the $Al_{100}P_XCe_Y$ solids. 0%P (solid line), 5%P (doted line), 10%P (dashed line) and 20%P (dashed-dotted line).

powders were pressed firmly into carved stainless steel holders so that they could be introduced into the ultra high vacuum (UHV) chamber. The UHV system (base pressure 8×10^{-10} mbar) consists of a fast entry assembly and the preparation and the analysis chambers. The latter was equipped with a hemispherical analyser (SPECS LH-10) and a twin-anode X-ray gun. The unmonochromatized Mg-Kα line at 1253.6 and a constant pass energy (97 eV) for the analyser were used for the analysis measurements.

Although the samples were grounded, due to their low electrical conductivity the excitation current caused by the X-ray irradiation of the sample surface resulted in the development of positive electrical charge on the surface. This caused a shift of the X-ray photoelectron spectra which were subsequently corrected. Carbon deposits on the surface were used as reference, considering that the binding energy of graphitic carbon is located at 284.6 eV. The spectral analysis was performed with the aid of the "XPS peak" software which was mainly used for deconvolution of the multiple peaks. The composition was calculated by considering a homogeneous system at the surface layers, considering the analyser transmission function, the inelastic mean free paths and the atom densities of the elements. Typical spectra for the peaks due to Al_{2p}, P_{2s} and Ce_{3d} are shown in Fig. 5.

Results

XRD data

The XRD results, shown in Fig. 1, indicate that the addition of phosphorus and/or cerium influences the final solids quite differently. The addition of phosphorus to the parent γ-Al_2O_3 (sample $Al_{100}P_0Ce_0$) transforms it into a rather amorphous solid (samples $Al_{100}P_5Ce_0$, $Al_{100}P_{10}Ce_0$, $Al_{100}P_{20}Ce_0$) for reasons which have been discussed previously.[31–33] Namely, the added phosphate groups are bound to aluminate species and prohibit the development of large crystallites of alumina, while at the same time they are not present in a large enough concentration for the formation of aluminium phosphate crystallites. The behaviour of cerium is totally different. Even at 5% addition (sample $Al_{100}P_0Ce_5$) it remains in a completely separated and well-crystallised phase of CeO_2, which is apparent in all the samples $Al_{100}P_XCe_Y$ ($Y > 0$). The only effect brought about by the addition of phosphorus, in the form of phosphates, is the gradual formation of the $CePO_4$, especially in the sample $Al_{100}P_{20}Ce_{20}$.

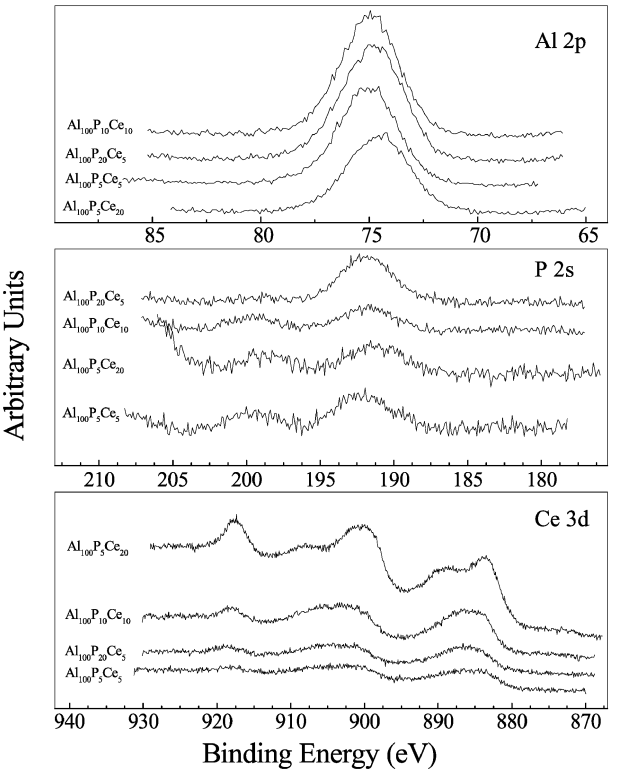

Fig. 5 Typical XPS spectra for the Al_{2p}, P_{2s} and Ce_{3d} shells in the $Al_{100}P_XCe_Y$ solids.

The size, d, of the CeO_2 crystallites was calculated using the Sherrer relationship

$$d = \frac{0.9\ \lambda}{b \cos \theta} \quad (1)$$

where d is the crystallite diameter in Å, λ is the wavelength in Å, θ is the Bragg angle in degrees and b is the observed peak width at half-maximum peak height in rads. The results are summarised in Fig. 3(f), which also shows some other characteristics of the solids.

Surface area and porosity

The adsorption–desorption isotherms of N_2 at $T = 77$ K and the calculated pore size distributions, shown in Fig. 2, indicate the influence of phosphorus and/or cerium on the porosity of the solids.

In Table 1, the specific surface area S (BET, $m^2\ g^{-1}$), the specific pore volume V_P (BJH, $cm^3\ g^{-1}$) and the mean pore diameter d_p ($d_p = 4V_P/S$, nm) are shown. Some of these parameters are shown in Fig. 3 as a function of phosphorus and cerium content.

Surface acidity

The acidity of the solids is shown in Fig 3(d) and (e) per g and per m^2 respectively. The acidity per m^2 increases linearly on addition of phosphates but is not affected by the addition of cerium. The TPD signals of NH_3 shown in Fig. 4 indicate three distinct peaks, one at around 180–200 °C, a second in the range 280–300 °C and a final one around 350–400 °C. These peaks should correspond to weak, medium and strong acid sites, respectively, the number of which can be quantified by deconvolution of the TPD signal. Typical results using a suitable Peakfit PC program and Gaussian components are shown in Fig. 6.

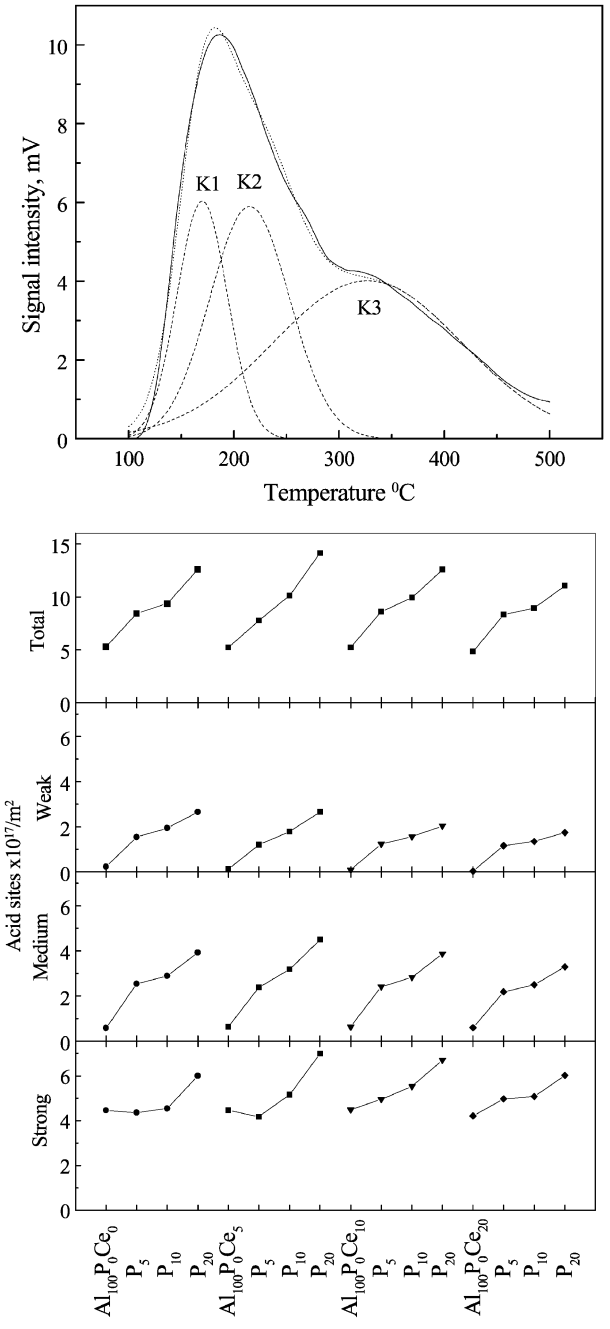

Fig. 6 Upper part: Deconvolution of a typical NH_3 TPD signal from Fig. 4 (sample $Al_{100}P_{20}Ce_0$). The K_1, K_2 and K_3 components correspond to weak, medium and strong acid sites respectively. Their development as a function of the composition of the solids is shown in the lower part, which also includes the total number of sites.

In the lower part of the Fig. 6 the mean surface density of the weak, medium and strong acid sites is shown as a function of the nominal composition of the solids.

XPS analysis

The surface composition of the solids, as determined by suitable treatment of the XPS spectra (Fig. 5) is shown in Table 2. The surface composition was deduced from the area of the corresponding peak as follows:[36] first the background type Shirley was subtracted; then from this corrected peak, which corresponds to the amount of each element in the surface, we calculated the relevant atomic ratios using the atomic sensitivity factors according to the formula

Table 2 Surface composition of the $Al_{100}P_XCe_Y$ solids as determined by XPS and the % enrichment or % depletion of the surface in phosphorus and cerium relative to the nominal composition from synthesis

Nominal sample composition from synthesis	XPS surface composition	% Enrichment in P	% Enrichment in Ce
$Al_{100}P_0Ce_0$	$Al_{100}P_0Ce_0$	—	—
$Al_{100}P_5Ce_0$	$Al_{100}P_{5.02}Ce_0$	0.42	—
$Al_{100}P_{10}Ce_0$	?	?	—
$Al_{100}P_{20}Ce_0$	$Al_{100}P_{21.1}Ce_0$	5.5	—
$Al_{100}P_0Ce_5$	$Al_{100}P_0Ce_{12.5}$	—	149.1
$Al_{100}P_5Ce_5$	$Al_{100}P_{6.2}Ce_{8.1}$	23.6	62.2
$Al_{100}P_{10}Ce_5$	$Al_{100}P_{13.4}Ce_{8.6}$	33.6	72.4
$Al_{100}P_{20}Ce_5$	$Al_{100}P_{22.3}Ce_{8.3}$	11.7	65.1
$Al_{100}P_0Ce_{10}$	$Al_{100}P_0Ce_{20.3}$	—	102.6
$Al_{100}P_5Ce_{10}$	$Al_{100}P_{5.8}Ce_{17.3}$	15.6	73.3
$Al_{100}P_{10}Ce_{10}$	$Al_{100}P_{11.5}Ce_{13.2}$	14.9	31.9
$Al_{100}P_{20}Ce_{10}$	$Al_{100}P_{23.4}Ce_{13.2}$	17.1	31.7
$Al_{100}P_0Ce_{20}$	$Al_{100}P_0Ce_{43.0}$	—	114.9
$Al_{100}P_5Ce_{20}$	$Al_{100}P_{4.3}Ce_{39.2}$	−13.9	96.2
$Al_{100}P_{10}Ce_{20}$	$Al_{100}P_{7.7}Ce_{32.4}$	−22.8	62.2
$Al_{100}P_{20}Ce_{20}$	$Al_{100}P_{16.3}Ce_{33.7}$	−18.7	68.7

$$\frac{I_A}{I_B}\frac{I_B^\infty}{I_A^\infty} = \frac{X_A}{X_B}\left[\frac{a_A}{a_B}\right]^3\frac{\lambda_B}{\lambda_A} \qquad (2)$$

where X_A/X_B is the atomic ratio of elements A and B on the surface, I_A/I_B is the ratio of the corrected peaks of photoelectrons of the same element, $\lambda = 0.054\sqrt{E_{KIN}}$ is the mean free path of photoelectrons, E_{KIN} is the corresponding kinetic energy in eV, I_A^∞, I_B^∞ are the empirically derived atomic sensitivity factors relative to the F 1s electronic state and finally, a_A, a_B are the atom sizes in Å. Table 2 contains the nominal formula as assumed from the synthesis and the actual surface formula as found by XPS. In the last two columns the observed % enrichment or % depletion is shown. As a basis of calculation we considered the aluminium atoms to be equal to 100 in both cases. We mentioned that for the Ce 3d, we took into account the corrected area of all peaks of the corresponding spectrum included the satellites, using an atomic sensitivity factor equal to 10. Thus a factor is given for metallic Ce and according to the literature this does not show appreciable difference from the corresponding sensitivity factor for CeO_2 and possibly for Ce_2O_3.

Discussion

Structure area, pore volume and surface acidity of the solids

The physicochemical properties of $Al_{100}P_xCe_y$ solids, are shown in 3D bar charts in Fig. 3. In this figure the following properties are drawn as a function of X and Y expressing the content of P and Ce in the solids: specific surface area, pore volume, mean pore diameter, surface acidity per g and per m^2 as well as the mean particle size of CeO_2 crystallites.

Let us discuss in detail the properties of the solids and their variation with X (%P) and Y (%Ce).

From Fig. 3(a) we observe that the addition of phosphorus at 5 and 10% levels increases substantially the specific surface area (S) of the samples from around 200 $m^2\ g^{-1}$ to 350–380 $m^2\ g^{-1}$. The enhancement of S is especially noticeable in the absence of or for low content of cerium. On the contrary cerium acts antagonistically to phosphorus decreasing the S of

the samples but its influence is moderated by the presence of phosphates.

From Fig. 3(b) we can see that the pore volume V_p increases with the addition of phosphorus and reaches values up to ~1 $cm^3\ g^{-1}$ for the $Al_{100}P_{20}Ce_{10}$. But the samples containing 20% cerium show substantially lower pore volume 0.30–0.35 $cm^3\ g^{-1}$. The mean pore diameters d_p, shown in Fig. 3(c), vary substantially with the addition of phosphates and cerium. At 0% addition of phosphorus the mean pore diameter is almost constant and around 6 nm for all amounts of cerium. As the phosphorus content increases, the mean pore diameter increases and reaches values d_p = 15–15.5 nm at 20% phosphorus and 5 and 10% cerium. The mean pore diameters of the samples with 20% cerium are somewhat smaller, between 6 and 8 nm. This effect is most probably due to the formation of $CePO_4$ which binds some phosphate groups, thus decreasing their availability for interaction with the aluminate groups.

The addition of phosphorus, apart from the strong influence in increasing the surface area, results also in a large increase in the number of acid sites, not only per g but also per m^2 of solids. This should be the result of phosphate groups which are attached on the surface of alumina species increasing thus the acidity according to the schemes shown in Fig. 7.[31–33]

It is of interest to observe that the addition of phosphorus increases much more effectively the medium and the weak acid sites. This in turn means that the strong acidity is due to the original Al_2O_3 and the new acid sites developed by the addition of phosphorus according to the schemes in Fig. 7 are mainly medium and weak ones (see Fig. 6). So it is apparent that the addition of phosphorus increases both the SSA and the surface acidity. A relevant question is whether the increase in surface acidity is proportional to the increase in the surface area. In other words if every time the surface area increases, and new phosphate groups are present on it, then, is the surface acidity due to these groups proportional to the new surface area. An answer to this question is attempted by comparing the following ratios

$$\frac{\text{surface acidity of } Al_{100}P_XCe_Y \text{ sample}}{\text{surface acidity of } Al_{100}P_0Ce_0 \text{ sample}} = \text{I} \qquad (3)$$

and

$$\frac{\text{surface area of } Al_{100}P_XCe_Y \text{ sample}}{\text{surface area of } Al_{100}P_0Ce_0 \text{ sample}} = \text{II} \qquad (4)$$

The ratio (I)/(II) provides some indication as to whether the increase in acidity and surface area are due to same reason, *i.e.* the addition of phosphorus, and if not, which sample is different. The ratios (I) and (II) as well as their own ratio (I)/(II) are shown in Fig. 8.

It can be seen that for samples $Al_{100}P_0Ce_0$, $Al_{100}P_5Ce_0$ and $Al_{100}P_{10}Ce_0$ the relative increase in acidity is similar to the increase in SSA. The same is almost true for samples $Al_{100}P_0Ce_5$ and $Al_{100}P_5Ce_5$. For the remaining samples, having a total number of heteroatoms $(X+Y) \geqslant 15$, this dependence ceases and the *relative acidity increases much faster, and independently of the surface area*. Or, otherwise, the surface area decreases as the addition of larger amounts of phosphorus and/or cerium results in the formation of crystalline phases of $AlPO_4$ and/or $CePO_4$, as indeed seen by the XRD data in Fig. 1.

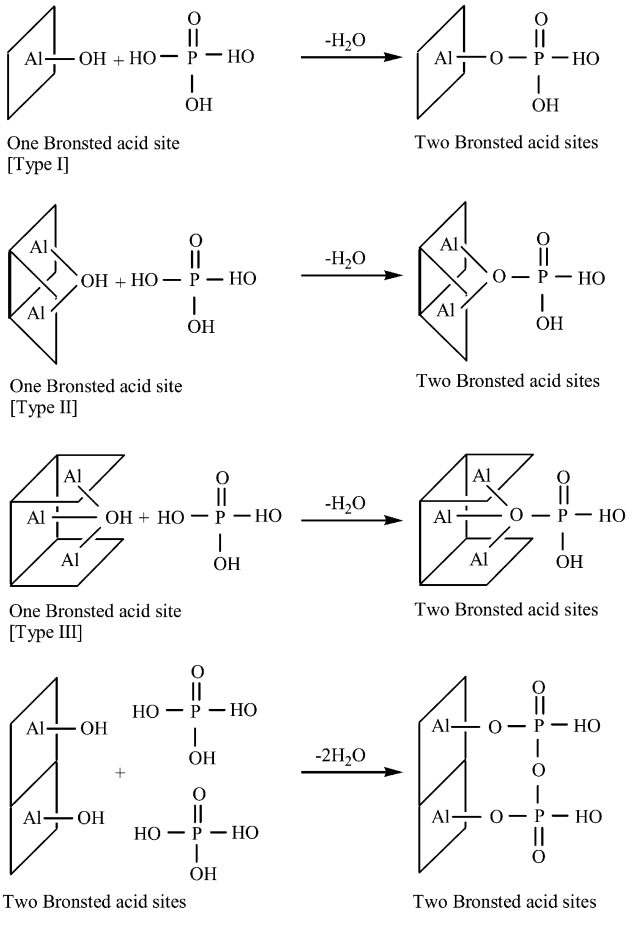

Fig. 7 Possible schemes for the increase in acid sites in alumina upon addition of phosphate groups.

Surface composition, crystallinity and acidity of the samples

The CeO_2 crystallites, as seen from the XRD, have a size around 6–6.5 nm in the samples without phosphorus ($Al_{100}P_0Ce_Y$) with a tendency to increase with increasing cerium content. The addition of phosphorus at the 5 and 10% levels, results in a decrease in the size of the CeO_2 crystallites to 4–4.5 nm (samples $Al_{100}P_5Ce_5$, $Al_{100}P_{10}Ce_5$) but also to

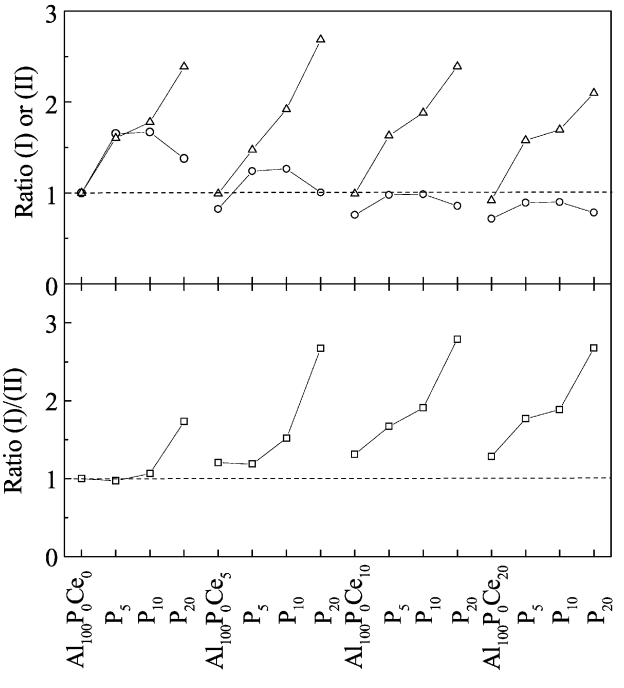

Fig. 8 Upper part: (△) Ratio I (eqn. (3)) of the surface acidity of each $Al_{100}P_XCe_Y$ sample over the surface acidity of the parent sample $Al_{100}P_0Ce_0$; (○) Ratio II (eqn. (4)) for SSAs. Lower part: (□) the ratio (I)/(II) showing the relative increase in acidity compared to the increase in surface area. The dotted horizontal lines at the point 1 are a guide for the eye.

an increase in their sizes to 7.5–8 nm for the samples with high cerium content ($Al_{100}P_5Ce_{20}$, $Al_{100}P_{10}Ce_{20}$). On the other hand, the addition of 20% phosphorus results in smaller crystallites of CeO_2, even at high cerium content (size ~5 nm for samples $Al_{100}P_{20}Ce_{10}$ and $Al_{100}P_{20}Ce_{20}$). These results can be explained if we assume that some of the phosphorus added is bound to cerium as $CePO_4$ and as a result the development of the CeO_2 phase is inhibited. This inhibition effect is maximized at low cerium and/or high phosphorus contents as expected and, therefore, the largest CeO_2 crystallites survive at high cerium and low phosphorus content (samples $Al_{100}P_5Ce_{20}$, $Al_{100}P_{10}Ce_{20}$). Nevertheless it not clear why small addition of phosphorus (5–10%) increase the size of the CeO_2 crystallites. Perhaps this effect is related to the substantial increase in surface area observed for these samples (compare Fig. 3(a) with Fig. 3(f)).

The surface composition of the samples for aluminium, phosphorus and cerium as probed by the XPS experiments, is summarised in Table 2. In the same table, the % enrichment, or % depletion in those elements is shown, relative to the nominal composition of the as-synthesised solids.

The most striking effect is the considerable enrichment of the surface in cerium. For samples with $Y = 5$ the enrichment is between 62% and 149%, for $Y = 10$ the enrichment is somewhat lower (between 31% and 102%) and for $Y = 20$ the enrichment rises again to between 62% and 114%. A second observation is that the % surface enrichment in cerium is reduced by the presence of phosphorus. Although this effect of phosphorus is differentiated in the subgroups with 5%, 10% and 20% cerium, a general relation for the 12 samples belonging to those three groups is as follows.

$$\text{Log(\% enrichment in Ce)} = 2.0305 - 0.0165(\%\text{P content by XPS}) \quad (5)$$

with a correlation coefficient $r = 0.8070$ which is better than 95% confidence limits. In effect this relation describes in a quantitative statistical way, how the enrichment of the surface in Ce is affected by the presence of phosphorus, as determined by XPS. For example, if %P (XPS) = 10% then log(%enrichement in Ce) = 2.0305 – 0.165 = 1.8655, or the enrichment in Ce is 73.4% on average. This should be compared with an average of about $10^{2.035} = 108.4\%$ in the absence of phosphorus. This effect of phosphorus should be due to the binding of phosphate groups with cerium to give $CePO_4$, which is also detected by the XRD data at high cerium and phosphorus content (Fig. 1). As discussed previously, the size of the CeO_2 crystallites is reduced on addition of phosphorus, presumably because some CeO_2 is transformed to $CePO_4$. A corroborative observation is the variation of the intensity of the main XRD reflection I_{main} of CeO_2 at $2\Theta \approx 28.7°$ with the % cerium surface content determined by XPS. This relation is shown in Fig. 9 and is described by an equation of the form.

$$I_{main}/I_{main,max} = [K(\%\text{Ce on the surface}]/[1 + K(\%\text{Ce on the surface})] \quad (6)$$

with a correlation coefficient $r = 0.9840$ which is better than 99% confidence limits, where $I_{main,max} = 1083.4$ and $K = 0.0908$.

Thus eqn. (6) expresses the fact that when the samples contain high % cerium on their surface, this cerium cannot actually remain in the form of CeO_2 but is transformed into some other chemical species, presumably $CePO_4$ in nanoparticle form, not detectable by XRD.

Finally some comments are in order relevant to the surface content in phosphorus as determined by XPS (Table 2) and the surface acidity as determined by the NH_3 TPD experiments. The relation between these two quantities is depicted in Fig. 10 and described by the relationship:

$$\text{Acid sites m}^{-2} = 5.778 \times 10^{17} + 0.338 \times 10^{17}(\%\text{P})_{XPS} \quad (7)$$

with a correlation coefficient $r = 0.9416$ which is better than 95% confidence limits.

This relationship (7) should be compared with the less precise relationship between acidity and the %P from the nominal composition of the solids, *i.e.* the X values.

$$\text{Acid sites m}^{-2} = 5.793 \times 10^{17} + 0.355 \times 0^{17}(\%\text{P})_{nominal} \quad (8)$$

with a correlation coefficient $r = 0.9132$ which is worse than that found by eqn. (7). Thus the XPS results provide much more precise information about the surface acidity generated by the phosphate groups according to Fig. 7. Such data can be very informative when dealing with the catalytic performance of such solids in a dehydration reaction as will be dealt with in a relevant future work.

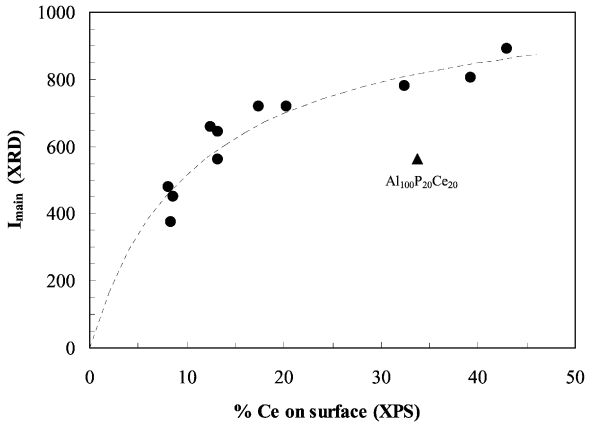

Fig. 9 Variation of the relative intensity of CeO_2 main peak (I_{main}) from XRD data (Fig. 1) over the intensity of the main peak for the sample $Al_{100}P_0Ce_{20}$ ($I_{main,max}$) with the % surface composition of cerium as found by XPS. The dashed line is described by eqn. (6).

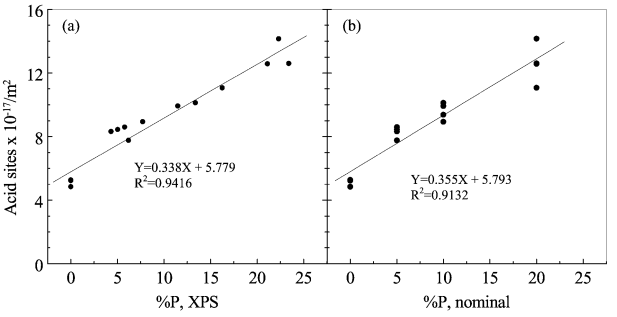

Fig. 10 Relationship between the number of acid sites per m^2 and the (%P) on the surface as determined by XPS (a) and the (%P) of the nominal composition of samples (b) (eqn. (7) and (8) respectively).

Conclusion

High surface area mesoporous cero-phosphoro-aluminate solids with the general formula $Al_{100}P_XCe_Y$ ($X,Y =$ 0,5,10,20) have been prepared. The surface area and the acidity are strongly and positively affected by the addition of phosphorus to the parent compound Al_2O_3. Phosphate groups are extensively accumulated at the surface (15–20%) at low ($Y < 20$) cerium content, while at high cerium content ($Y = 20$) a depletion of phosphorus (15–20%) is observed. Cerium is extensively accumulated on the surface (30–150%) but its accumulation is lowered by the presence of phosphorus.

The addition of phosphorus generates mainly middle and weak new acid sites, while the strong acidity seems to be due mainly to the parent γ-alumina.

References

1 A. Trovarelli, *Catal. Rev.-Sci. Eng.*, 1996, **38**, 439.
2 J. C. Summers and S. A. Ausen, *J. Catal.*, 1979, **58**, 131.
3 G. Kim, *Ind. Eng. Chem. Prod. Res. Dev.*, 1982, **21**, 267.
4 H. S. Gandhi, A. G. Piken, M. Shelef and R. G. Delosh, *SAE Paper 7760201*, 1976, p. 55.
5 J. F. Brazdil and R. K. Grasselli, *J. Catal.*, 1983, **79**, 104.
6 W. Liu and M. Flytzani-Stefanopoulos, *J. Catal.*, 1995, **153**, 304.
7 S. Imamura, Y. Uematsu, K. Utani and T. Ito, *Ind. Eng. Chem. Res.*, 1991, **30**, 18.
8 F. Zamar, A. Trovarelli, C. de Leitenburg and G. Dolcetti, *J. Chem. Soc. Chem. Commun.*, 1955, 965.
9 Z. Yu, X. Yang, J. H. Lunsford and M. P. Rosynek, *J. Catal.*, 1995, **154**, 163.
10 M. Haneda, T. Mizushima, N. Kakuta, A. Ueno, Y. Sato, S. Matsuura, K. Kasahara and M. Sato, *Bull. Chem. Soc. Jpn.*, 1993, **66**, 1279.
11 A. A. Bhattacharyya, G. M. Woltermann, J. S. Yoo, J. A. Karch and W. E. Cormier, *Ind. Eng. Chem. Res.*, 1988, **27**, 1356.
12 M. Shelef and G. W. Graham, *Catal. Rev.-Sci. Eng.*, 1994, **36**, 433.
13 J. T. Kummer, *J. Phys. Chem.*, 1986, **90**, 4747.
14 K. C. Taylor, *Catal. Rev.-Sci. Eng.*, 1993, **35**, 457.
15 R. K. Herz, *Ind. Eng. Chem. Prod. Res. Dev.*, 1981, **20**, 451.
16 L. L. Hegedus, J. C. Summers, J. C. Schlatter and K. Baron, *J. Catal.*, 1979, **56**, 321.
17 A. F. Diwell, R. R. Rajaram, H. A. Shaw and T. J. Truex, *Stud. Surf. Sci. Catal.*, 1991, **71**, 139.
18 G. Munuera, A. Fernandez and A. R. Gonzales-Elipe, *Stud. Surf. Sci. Catal.*, 1991, **71**, 207.
19 M. S. Brogan, T. J. Dines and J. A. Cairns, *J. Chem.Soc., Faraday Trans.*, 1994, **90**, 1461.
20 J. Z. Shyu, K. Otto, W. L. H. Watkins, G. W. Graham, R. K. Belitz and H. S. Gandhi, *J. Catal.*, 1988, **114**, 23.
21 S. Bernal, F. J. Botana, J. J. Calvino, G. A. Cifredo, J. A. Perez-Omil and J. M. Pintado, *Catal. Today*, 1995, **23**, 219.
22 J. Z. Shyu and K. Otto, *J. Catal.*, 1989, **115**, 16.
23 L. L. Murel, S. J. Tauster and D. R. Anderson, *Stud. Surf. Sci. Catal.*, 1991, **71**, 275.
24 S. Bernal, G. Blanco, J. J. Calvino, G. A. Cifredo, J. A. P. Omil, J. M. Pintado and A. Varo, *Stud. Surf. Sci. Catal.*, 1994, **82**, 507.
25 Z. R. Ismagilov, R. A. Shkrabina, N. A. Koryablina and F. Kapteijn, *Catal. Today*, 1995, **24**, 269.
26 B. Harrison, A. F. Diwell and C. Hallett, *Platinum Metals Rev.*, 1988, **32**, 73.
27 M. Ozawa and M. Kimura, *J. Mater. Sci. Lett.*, 1990, **9**, 291.
28 C. Morterra, G. Magnacca, V. Bolis, M. Baricco, A. Giachello and M. Fucale, *Proceedings of the International Conference CAPoC 3*, Brussels, 1994, vol. 2, p. 225.
29 H. C. Yao and Y. F. Y. Yao, *J. Catal.*, 1984, **86**, 254.
30 V. R. Choudhary and V. H. Rane, *J. Catal.*, 1991, **130**, 411.
31 D. E. Petrakis, P. J. Pomonis and A. T. Sdoukos, *J. Chem. Soc., Faraday Trans.*, 1991, **87**(6), 901.
32 D. E. Petrakis, P. J. Pomonis and A. T. Sdoukos, *J. Chem. Soc., Faraday Trans.*, 1991, **87**(9), 1439.
33 D. E. Petrakis, M. J. Hudson, P. J. Pomonis, A. T. Sdoukos and T. V. Bakas, *J. Mater. Chem.*, 1995, **5**(11), 1975.
34 D. E. Petrakis, I. Pasxalidis, C. R. Theocharis, M. J. Hudson and P. J. Pomonis, *J. Colloid interface Sci.*, 1997, **185**, 104.
35 K. M. Kolonia, D. E. Petrakis, T. N. Angelidis, P. N. Trikalitis and P. J. Pomonis, *J. Mater. Chem.*, 1997, **7**(9), 1925.
36 *Practical Surface Analysis*, vol. 1, ed. D. Briggs and M. P. Seah, Wiley, New York, 1990.